ELSEVIER

Microelectronics Journal 39 (2008) 711–716

Microelectronics Journal

www.elsevier.com/locate/mejo

Center embossed diaphragm design guidelines and Fabry–Perot diaphragm fiber optic sensor

Yan Sun[a,*], Ganhua Feng[a], George Georgiou[a], Edip Niver[a], Karen Noe[b], Ken Chin[a]

[a]*New Jersey Institute of Technology, Department of Physics, Tiernan Hall, Newark, NJ 07102, USA*
[b]*PSE&G Corporation, (T-10A) 80 Park Plaza, P.O. Box 570, Newark, NJ 07102, USA*

Received 2 November 2007; accepted 15 December 2007
Available online 07 February 2008

Abstract

This research established the design guidelines for center embossed diaphragms for micro-diaphragm fiber type sensors. Following the guidelines, a center embossed diaphragm fiber optic sensor (CE-DFOS) based on Fabry–Perot interference was designed and fabricated with micro-electro-mechanical system (MEMS) technology. The CE-DFOS was experimentally verified to have the designed intrinsic frequency, and demonstrated high sensitivity in parallel testing with a piezoelectric (PZT) sensor.

Keywords: Center embossed diaphragm; Fabry–Perot; Fiber optic; Acoustic sensor; MEMS

1. Introduction

Diaphragm fiber optic sensors (DFOS) are Fabry–Perot interferometric devices, which are based on the interference of multiply reflected beams modulated by the change of the diaphragm-fiber gap induced by the signals being measured. An ideal DFOS should have high sensitivity, small size, chemical resistance, and immunity to electromagnetic interference (EMI) caused noise. In recent years much effort has been made to develop DFOS for static pressure and acoustic signal detection [1–4]. There are, however, still some limitations in these first generation DFOS sensors [5]. First of all, the distance between the optical fiber tip and the diaphragm is about 10 times greater than the diameter of the fiber core. Efficiency is low because most of the light is lost when it is first reflected from the diaphragm. Second, the existing macroscopic assembling methods of the devices are susceptible to axial, lateral, and angular misalignment, further adding to the loss of light and low efficiency. More severely, misalignment causes uncertainty of the intensity of the light reflected back to the fiber. Multi-fringe interference is complicated even more by the non-linear relationship between the deflection of the diaphragm and the signal being measured. As a result, reliability and Q-point (the linear, most sensitive operation point) stability have not been achieved in the first generation DFOS [5,6].

Many potential improvements in sensor performance can be realized by using a center embossed diaphragm in DFOS by micro-electro-mechanical system (MEMS) fabrication. Firstly, the embossed center minimizes the impact of potential lateral misalignment between the fiber and the diaphragm, and the precision of MEMS technology reduces the possibility of axial, lateral, and angular misalignment. Secondly, with MEMS technology, the gap between the center embossment and the fiber end can be shortened to be as little as several micrometers for near field operation to improve efficiency. Thirdly, while the gap between the embossed center and the fiber tip is only a few micrometers, the distance between the diaphragm base and the fiber tip can be considerably larger. This geometry provides a larger air cavity volume, which reduces the air cavity back pressure that impedes diaphragm movement and sensitivity. All of these improvements enable the sensor to work stably at Q-point, achieving linear and most sensitive operation afforded by the Fabry–Perot mechanism. Recently we reported the first center embossed DFOS and the first static testing experiment that verified the

*Corresponding author. Tel.: +1 973 342 2616; fax: +1 973 596 5794.
E-mail address: ys2@njit.edu (Y. Sun).

0026-2692/$ - see front matter © 2008 Elsevier Ltd. All rights reserved.
doi:10.1016/j.mejo.2007.12.020

DFOS sensor to be a truly and purely Fabry–Perot interferometric device [7].

The performance characteristics of a diaphragm are affected by its shape, size, and presence or absence of embossment. Although the guidelines for designing flat diaphragms are well established [8], the design guidelines for center embossed diaphragms have yet to be systematically investigated. A goal of this research is to establish the design guidelines for center embossed diaphragms by characterizing the relationship between the shape and size of the embossment, the shape and size of the diaphragm, center deflection, sensitivity, and intrinsic frequency. Another goal is to design and fabricate a center embossed DFOS (CE-DFOS) according to the guidelines. A third goal is to experimentally verify that the CE-DFOS performs as it is designed to, and that it achieves high efficiency and sensitivity.

2. Diaphragm design guidelines

The two most important characteristics of a diaphragm are center deflection and frequency response. The ideal diaphragm response should be linear and most sensitive to the signal at its intrinsic frequency. The structure geometry of a center embossed diaphragm is shown in Fig. 1, where H and h are the thickness of the diaphragm and the embossment, a and b are the radius of a circular diaphragm and its center embossment, or the half side length of a square diaphragm and its embossment.

2.1. Center deflection

Center deflection of an edge-clamped diaphragm as a function of applied pressure is widely used to calculate linearity and sensitivity in pressure and acoustic sensors. For a flat circular diaphragm with clamped edges, the center deflection (y_0) is analytically expressed as [8]

$$y_0 = \frac{Pa^4}{64D},$$

$$D = \frac{EH^3}{12(1-v^2)}, \tag{1}$$

where P is pressure, a is diaphragm radius, H is diaphragm thickness, E is Young's Modulus, v is Poisson's ratio, and D is flexural rigidity.

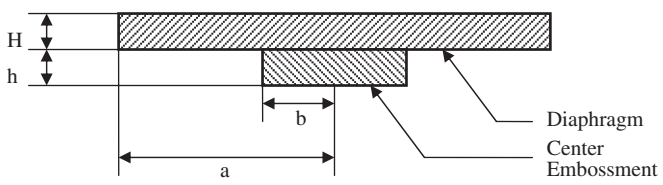

Fig. 1. Structure geometry of a center embossed diaphragm.

The sensitivity is defined as

$$S = \frac{\Delta y_0}{\Delta P}. \tag{2}$$

For a circular diaphragm, the center deflection of a center embossed diaphragm is analytically formulated as [9]

$$y_0 = \frac{A_p a^4}{EH^3} P,$$

$$A_p = \frac{3(1-v^2)}{16}\left(1 - \frac{b^4}{a^4} - 4\frac{b^2}{a^2}\log\frac{a}{b}\right), \tag{3}$$

where b is the radius of the embossment. The b/a ratio is a very important parameter affecting the performance characteristics of the center embossed diaphragm.

As shown in Fig. 2, a higher b/a ratio makes a stiffer diaphragm. The simulated results by Femlab (software, COMSOL Multiphysics 3.3) are in good agreement with the theoretical results from Eq. (3). The stiffness brought about by the embossed center reduces the deflection of the center embossed diaphragm under load. This makes response of the center embossed diaphragm to applied pressure more linear than that of the diaphragm without embossment. On the other hand, sensitivity decreases as b/a ratio increases. In order to minimize loss in sensitivity, the b/a ratio should be within 20%.

The center deflection of a flat square diaphragm with clamped edges is [8]

$$y_0 = \frac{Pa^4}{47D}. \tag{4}$$

The center deflection of a center embossed square diaphragm with clamped edges has no analytical solution, but can be numerically calculated with Femlab software.

The simulation results of sensitivity of a center embossed square diaphragm as the function of b/a ratio are shown in Fig. 3. Similar to the circular diaphragm, increasing b/a ratio decreases sensitivity of the square diaphragm. Comparing Fig. 2 with Fig. 3, a circular diaphragm is stiffer than a square one if they have the same thickness, and the side length of the square diaphragm is equal to the diameter of the circular one. As shown in Figs. 2 and 3, the

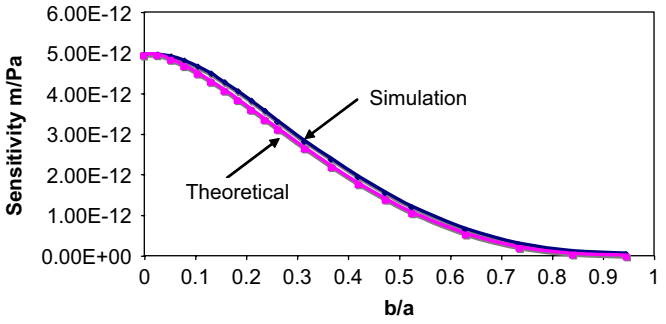

Fig. 2. Simulation and theoretical results of sensitivity of a circular diaphragm as a function of the b/a ratio, with a being a constant of 950 μm.

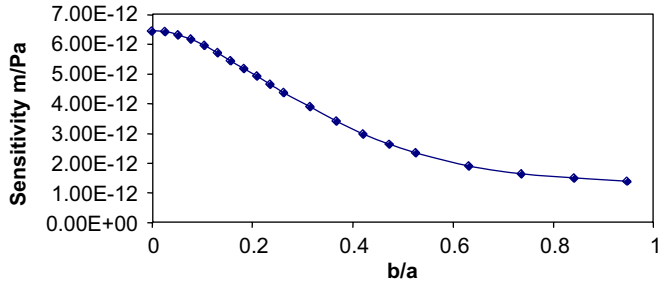

Fig. 3. Simulation results of the sensitivity of a square diaphragm as a function of the b/a ratio, with a being a constant of 950 μm.

square diaphragm is more sensitive than the circular counterpart. The designed sensitivity can be achieved by choosing the proper ratios of b/a and h/H.

2.2. Frequency response

Frequency response is another important consideration in design of acoustic sensors. The intrinsic frequency of a flat circular diaphragm is [10]

$$f = \frac{40.8H}{2\pi d^2}\sqrt{\frac{E}{12(1-v^2)\rho}}, \tag{5}$$

where g is gravitational constant, d is diameter of the diaphragm, ρ is density of the diaphragm material.

The intrinsic frequency of a square diaphragm is [9]

$$f = \frac{35.1H}{2\pi a^2}\sqrt{\frac{E}{12(1-v^2)\rho}}, \tag{6}$$

where a is side length of the square diaphragm.

Eqs. (5) and (6) indicate that a circular diaphragm has a higher intrinsic frequency than a square one if they have the same thickness, and the side length of the square diaphragm is equal to the diameter of the circular one.

Fig. 4 shows the relationship between the ratio h/H, b/a, and intrinsic frequency for a circular diaphragm. Fig. 5 shows a similar relationship for a square diaphragm. Increasing ratio b/a initially decreases the frequency because of the increasing inertia. Further increasing the b/a value progressively increases the frequency. After the b/a ratio passes a certain point, the intrinsic frequency of a thicker embossment (larger h/H) increases significantly faster than that of a thinner embossment (smaller h/H). Therefore, while adding center embossment will improve the linearity of the diaphragm response, a small b/a ratio offers the best compromise to achieve both high sensitivity and better response to high frequency. When b/a is at a small ratio of 0.184, the intrinsic frequency decreases as h/H increases. For a sensor to respond better to high frequency, the thickness of the embossment should not exceed the thickness of the diaphragm.

The guidelines discussed above apply to sensors in air, water or other media. A correction factor should be applied to the intrinsic frequency when it is in a medium

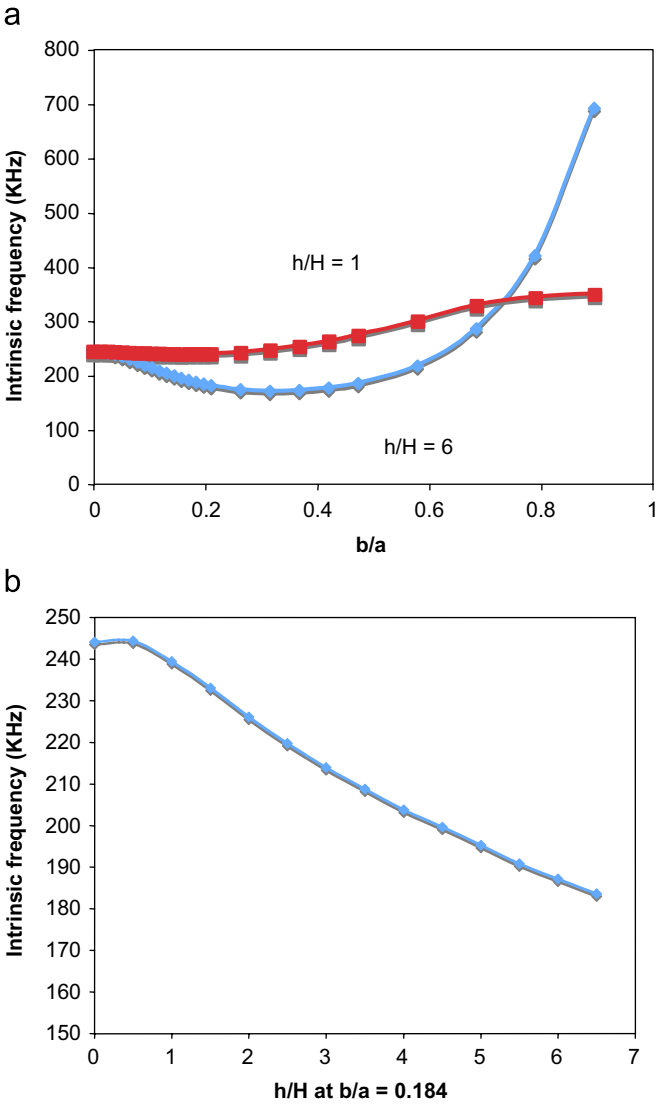

Fig. 4. Simulation results of intrinsic frequency of a circular diaphragm as a function of (a) ratio b/a, (b) ratio h/H.

other than air. The correction factor is calculated as [10]

$$\frac{1}{\sqrt{1+0.669(\rho_m a/\rho H)}}, \tag{7}$$

where ρ_m is the density of the medium, and ρ is the density of the diaphragm.

2.3. Diaphragm design for DFOS

Following the guidelines established above, the design parameters were calculated to fabricate an acoustic sensor with an intrinsic frequency of 100 kHz in water. A square diaphragm instead of a circular one was chosen in the design for its higher sensitivity and easier processability with MEMS technology. The calculations were performed via Femlab software simulation of the intrinsic frequency and center deflection of the center-embossed diaphragm, as shown in Fig. 6. According to the simulations, the sensor should have the following dimensions in order to achieve

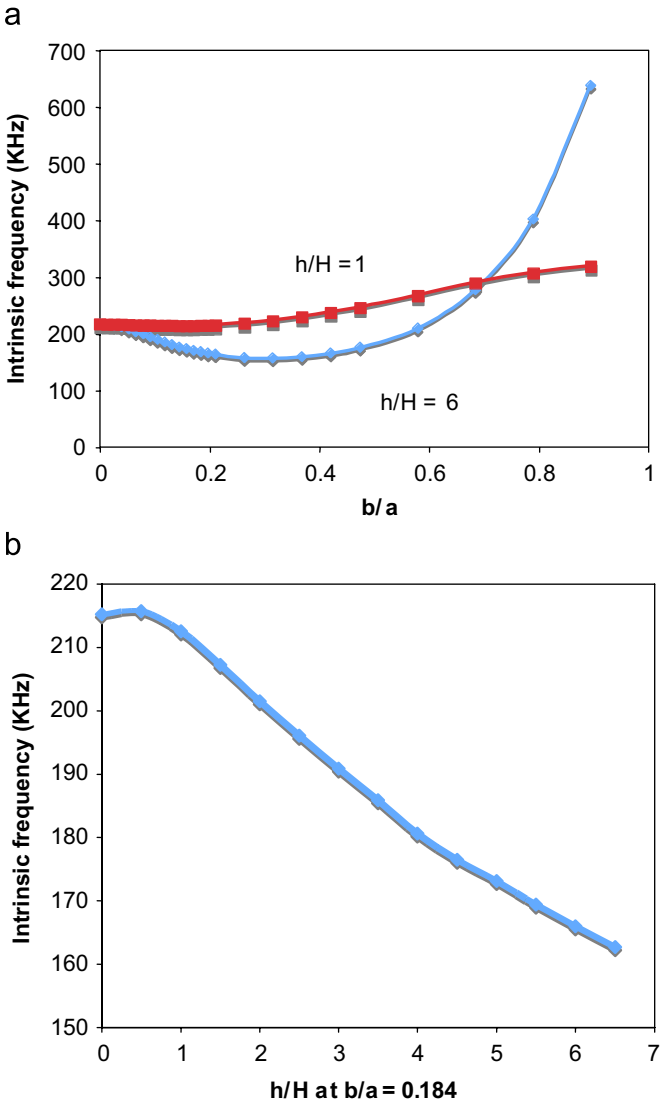

Fig. 5. Simulation results of intrinsic frequency of a square diaphragm as a function of (a) ratio b/a, (b) ratio h/H.

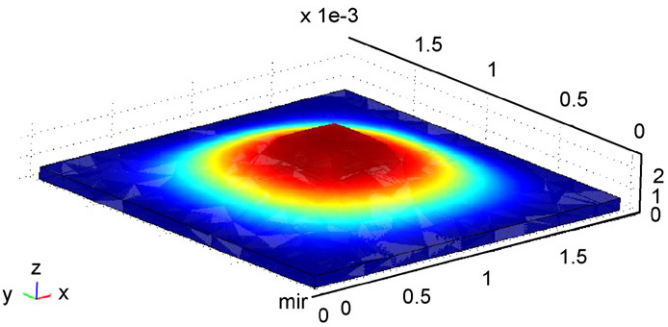

Fig. 6. A 3-D Femlab simulation of the center embossed square diaphragm for the DFOS.

an intrinsic frequency of 100 kHz: 1.9 mm of diaphragm side length, 60 μm of diaphragm thickness, 350 μm of embossment side length, and 60 μm of embossment thickness.

3. Sensor fabrication

The diaphragm was fabricated using MEMS technology. A 220-μm silicon wafer was etched down in KOH on each side sequentially to produce a 60-μm thick diaphragm. The embossed center was protected by a layer of silicon oxide to ensure that it remained intact in the etching process. As a result, both ends of the Fabry–Perot cavity (the embossed center and fiber tip) were perfect flat surfaces to reduce speckle noise. The surrounding wall on the embossed-center side of the diaphragm was coated with gold by evaporation. The gap between the embossed center and fiber end was accurately determined by the gold film thickness.

The diaphragm and fiber tip were first clamped together mechanically. The gap between the diaphragm and the fiber was then finely tuned while measuring the interference light signal output until it reached linear operation and the highest detection sensitivity, defined as Q-point. After the sensor operation had reached Q-point, the diaphragm and the fiber ferule were soldered together with Ag–Sn–Pb175 under microscope. The final gap between the center embossment and the fiber end was approximately 2 μm. The finished sensor is shown in Fig. 7.

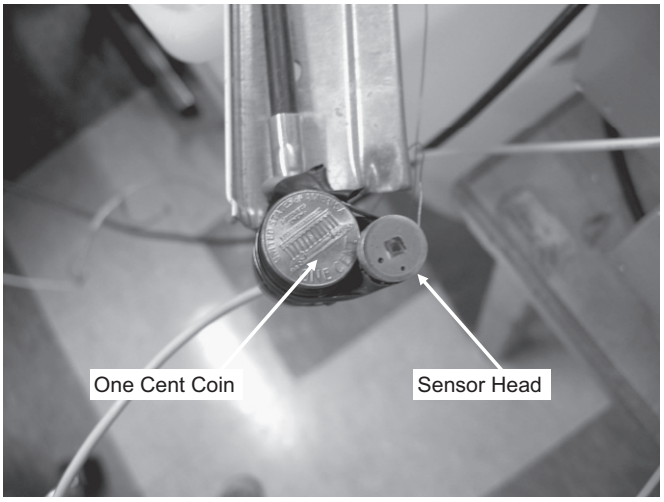

Fig. 7. Photograph of the fabricated DFOS.

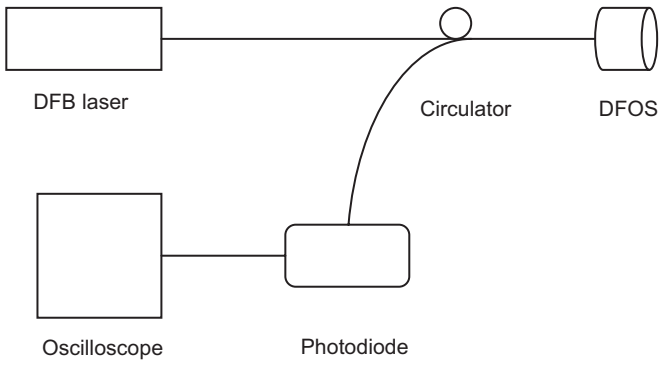

Fig. 8. Schematic of DFOS sensor characterization.

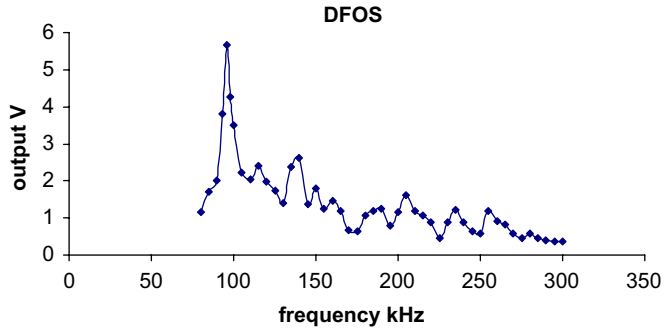

Fig. 9. Frequency response spectrum of the DFOS.

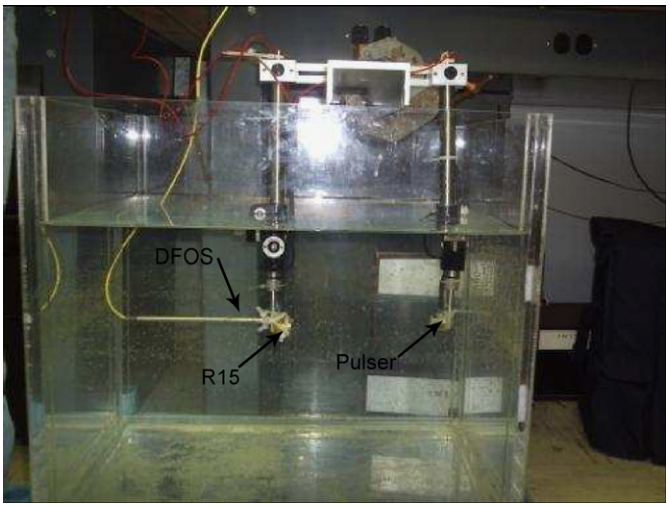

Fig. 10. Underwater parallel testing of the DFOS and PZT (R15) sensors.

4. Sensor testing results and discussions

The complete system for sensor characterization is schematically illustrated in Fig. 8. It consists of the fabricated DFOS, a 1527 nm DFB laser, a 3-port fiber circulator, a photodiode, and an oscilloscope. The light from the DFB laser propagates along the single mode fiber to the DFOS through the circulator and interferes inside the DFOS. The modulated light propagates back in the third leg of the circulator and is detected by the photodiode, which turns an optical signal into an electronical signal. The electronical signal is processed and collected by an oscilloscope to produce the signal output.

4.1. Dynamic pressure testing

The purpose of the dynamic pressure testing is to test the sensor's frequency response. The CE-DFOS ultrasonic sensor was tested in water with a piezoelectric sensor (PZT, Model R15, Physical Acoustic Corporation) being used as the calibrated sound source. A function generator (HP Model 3312A, 15 MHz) drove the PZT sensor at different voltage and frequency from 80 to 300 kHz. A GHz digital oscilloscope (Agilent, Model DSO6104A) was used for signal collection. The DFOS had sound signal responses in 80–300 kHz range. As shown in Fig. 9, the frequency spectrum of DFOS has a peak response at approximately 100 kHz, which is the designed intrinsic frequency of the sensor. In other words, the sensor performed exactly as it was designed to by following the guidelines established in this work.

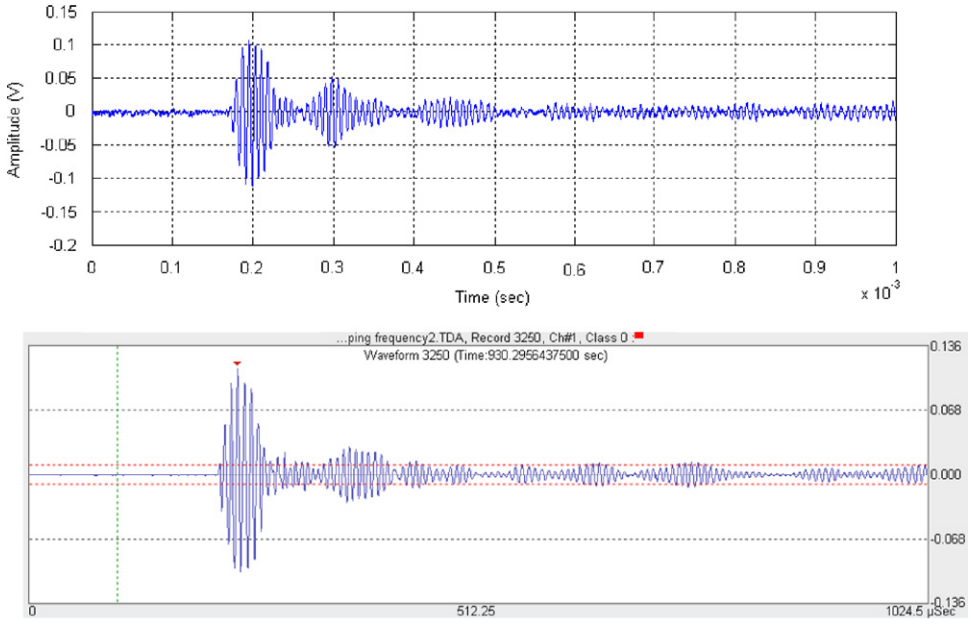

Fig. 11. Waveforms of the DFOS (top) and PZT (bottom) sensors.

4.2. Parallel testing with PZT sensor

PZT sensors have been the benchmark for acoustic detection. To test the sensitivity of the DFOS, it was tested in parallel with a PZT sensor (Model R15) with a 20 dB amplification circuit (a filter and 10 × amplification circuit) under identical conditions. The two sensors were immersed in water at the same distance away from an ultrasound pulser source, as shown in Fig. 10. The acoustic waves were created by another PZT (Model R15) as the pulser source placed approximately 8 in away from both sensors. The source frequency was increased from 75 to 300 kHz in 5 kHz increments. Fig. 11 shows the acoustic pressure response waveforms of the DFOS and PZT to a signal at 130 kHz. Both sensors exhibited very similar waveform profiles. Both the amplitude of the DFOS signal without any amplification and the amplitude of the PZT signal with 10 × amplification were approximately 200 mV. Very high efficiency and sensitivity of the DFOS as compared with PZT sensors was demonstrated.

5. Conclusions

The design guidelines for center embossed diaphragm have been established by characterizing the relationship between the size and shape of the embossment and the diaphragm, center deflection, sensitivity, and intrinsic frequency. A center embossed diaphragm fiber optic sensor based on Fabry–Perot interferometry was successfully designed and fabricated following the guidelines. The CE-DFOS achieved its designed intrinsic response of 100 kHz. It also showed high efficiency and sensitivity when compared with commercial PZT sensors.

Acknowledgments

The authors acknowledge helpful discussions with Dr. H. Lim, Mr. I. Padron, and Mr. H. Roman, as well as collaborations with Physical Acoustic Corporation. Funding for this research was provided by Public Service of Energy and Gas (PSE&G) and the Foundation of New Jersey Institute of Technology (NJIT).

References

[1] B. Yu, Fiber Fabry–Perot sensors for detection of partial discharges in power transformers, Appl. Opt. 42 (16) (2003) 3241.
[2] M. Yu, B. Balachandran, Sensor diaphragm under initial tension: linear analysis, Soc. Exp. Mech. (2005) 123.
[3] Y. Zhu, A. Wang, Miniature Fiber-Optic pressure sensor, IEEE Photonics Technol. Lett. 17 (2) (2005) 447.
[4] J. Xu, X. Wang, K. Cooper, A. Wang, Miniature all-silica fiber optic pressure and acoustic sensor, Opt. Lett. 30 (24) (2005) 3269.
[5] X. Wang, K. Farmer, An ultra-sensitive optic MEMS sensor for partial discharge detection, J. Micromech. Microeng. (2005) 521.
[6] A. Wang, Y. Liu, B. Ward, Prototype fiber-optic acoustic partial discharge sensor—lessons learned documentation and field test, EPRI Internal Technical Report (TR-1001768), 2002.
[7] K. Chin, Y. Sun, G. Feng, G. Georgiou, K. Guo, E. Niver, et al., Fabry–Perot diaphragm fiber optic sensor (DFOS), Appl. Opt. 46 (31) (2007) 7614.
[8] S.P. Timoshenko, S. Woinowski-Krieger, Theory of Plates and Shells, McGraw-Hill, New York, 1959, pp. 415–425.
[9] M. Bao, Analysis and Design Principles of MEMS Devices, Elsevier, Amsterdam, 2005, p. 101.
[10] M.D. Giovanni, Flat and Corrugated Membrane Design Handbook, Mercel Dekker Inc., New York, 1982, pp. 157–158.